*American Mineralogist, Volume 68, pages 517–529, 1983*

# Conditions of riebeckite formation in the iron-formation of the Dales Gorge Member, Hamersley Group, Western Australia

TAKASHI MIYANO[1] AND CORNELIS KLEIN

*Department of Geology*
*Indiana University*
*Bloomington, Indiana 47405*

**Abstract**

Quantitative evaluation of the stability relations of riebeckite, in the system Na–Fe–Mg–Si–C–O–H at low temperature and pressure, is based upon estimated thermodynamic parameters for riebeckite and on chemical and petrologic data. This evaluation forms the basis for an assessment of the conditions of riebeckite formation in the Dales Gorge Member, Hamersley Group, Western Australia. Computed values of $S^{\circ}_{298}$, $\Delta H^{\circ}_{f,298}$, $\Delta G^{\circ}_{f,298}$ for riebeckite are 657.3 J/mol K, −10058.30 kJ/mol, and −9365.2 kJ/mol, respectively. At constant temperature riebeckite is, in general, stable to lower $f_{O_2}$ conditions than hematite and higher pH values than magnetite or hematite. Where riebeckite coexists with carbonates, its stability field is enlarged by a decrease of total carbonate ($a_{\text{total } CO_2}$) at constant pH. Riebeckite assemblages in the iron-formations of the Dales Gorge Member can be divided into two groups, carbonate-free and carbonate-bearing. The former riebeckite has a high $X^{Rk}_{Fe}$ (ranging from 0.65 to 0.80) and the latter a much lower range from 0.40 to 0.55. The log $a_{Na^+}/a_{H^+}$ of riebeckite with such compositions ranges from 3.54 (for low $X^{Rk}_{Fe}$) to 3.69 (for high $X^{Rk}_{Fe}$) at 130°C and on the HM buffer. Because the $f_{O_2}$ for these iron-formations is almost fixed at the HM buffer, the conditions of riebeckite formation appear to have been controlled mainly by $a_{Na^+}$ and $a_{\text{total } CO_2}$ at a given temperature.

## Introduction

Several major Precambrian iron-formation sequences in the world contain abundant riebeckite and/or crocidolite which is of very low-grade metamorphic (or late diagenetic) origin. Major riebeckite and crocidolite (blue amphibole asbestos) deposits are well known in iron-formations of the Hamersley Group of Western Australia (*e.g.*, Trendall and Blockley, 1970) and the Transvaal Group of South Africa (*e.g.*, Beukes, 1973). Small amounts of riebeckite have also been reported from the Sokoman Iron Formation, Knob Lake area, Labrador Trough (*e.g.*, Zajac, 1974). In sedimentary rocks other than iron-formations, authigenic magnesio-arfvedsonite surrounding detrital hornblende was reported by Milton *et al.* (1974) in the Green River Formation. Similar authigenic textures also occur in the iron-formation of the Hamersley Group (Miyano, 1982).

The mineralogy and petrology of riebeckite-bearing iron-formations have been described by Hall (1930), Du Toit (1945), Genis (1964), Cilliers (1964), Beukes (1973, 1980) for the Transvaal Group; by Miles (1942), Trendall (1965, 1966), Trendall and Blockley (1970), Grubb (1971), Ayres (1972), Miyano (1976a, 1982), Klein and Gole (1981), Miyano and Miyano (1982) for the Hamersley Group; and by Dimroth and Chauvel (1973), Klein (1974), and Zajac (1974) for the Sokoman Iron Formation.

Ernst (1962) experimentally determined the stability field of riebeckite, which at relatively high temperature and pressure is bounded by the lower part of the stability field of acmite, at the hematite–magnetite (HM) buffer. Grubb (1971) showed, using experimental gel-runs that riebeckite may form at temperatures as low as 100–150°C and prefers low Eh and relatively low pH conditions.

The stability relations of riebeckite in very low-grade metamorphic (late diagenetic) iron-formations, however, have not been quantitatively assessed because of the lack of available thermodynamic data and on account of experimental difficulties. In this paper, we briefly describe some of the mineralogy, petrology, and chemistry of riebeckite within the Dales Gorge Member of the Hamersley Group, Western Australia, as an introduction to the evaluation of the stability relations of riebeckite using the estimated thermodynamic properties. We also discuss the physicochemical environment of riebeckite (crocidolite) formation during very low-grade metamorphism (or late diagenesis).

[1] Permanent address: Institute of Geoscience, University of Tsukuba, Ibaraki 305, Japan.

0003–004X/83/0506–0517$02.00

## Mineralogy and petrology

The Dales Gorge Member of the Brockman Iron Formation is a rock unit characterized by the most abundant riebeckite (crocidolite) among the various rock types of the Hamersley Group. Riebeckite is also known in the Joffre Member of the same sequence (above the Dales Gorge Member) and in the Marra Mamba Iron Formation, the lowest member of the Hamersley Group (Trendall and Blockley, 1970; Klein and Gole, 1981).

The mineralogy and petrology of the Dales Gorge Member rocks have been described by Miles (1942), Trendall (1965, 1966), Trendall and Blockley (1970), Grubb (1971), Ayres (1972), and Miyano (1976a). Recently Miyano (1982) and Miyano and Miyano (1982) reported the common occurrence of ferri-annite from riebeckite-bearing rocks of the Dales Gorge Member. This mineral appears to have been misidentified as ferri-stilpnomelane in earlier publications because of the optical and textural similarities of the two minerals. Ferri-annite is included in the reported mineral assemblages for such rocks, as shown in Table 1. It appears texturally that riebeckite and also ferri-annite formed later than other minerals (Trendall and Blockley, 1970; Ayres 1972; Miyano 1976a, 1982; Klein and Gole, 1981).

Table 1. List of riebeckite assemblages in banded iron-formations of the Dales Gorge Member, Hamersley Group, Western Australia

| Carbonate-free assemblages | mode of occurrence |
|---|---|
| Rk+Mt±Qtz±Py | (1),(2) |
| Rk+Hm±Mt±Qtz | (2) |
| Stil+Mica+Rk+Mt±Qtz | (3),(4) |
| Mica+Hm+Mt+Rk+Qtz | (4) |
| Qtz+Stil+Rk+Mi+Mt±Hm | (3) |
| Mt+Qtz+Mica+Rk | (4) |
| Carbonate-bearing assemblages | |
| Qtz+An+Mt+Hm+Rk | (4) |
| Qtz+Mica+Rk+Mt+Hm+An | (3),(4) |
| Qtz+An+Rk+Mt+Hm+Stil | (3),(4) |
| Rk+An(±Sd)±Py+Mt±Qtz±Stil | (2),(3) |
| Qtz+Hm+An+Rk±Mt | (4) |
| Qtz+Mt+Mica+Rk+Stil±An±Sd | (4) |
| An+Stil+Qtz+Mt+Rk±Py | (3) |
| Qtz+Hm+Mt+An+Rk+Mica | (4) |
| Qtz+Sd(±An)+Hm+Rk±Stil±Mt | (3),(4) |
| Qtz+Mt+Pho+Rk+Mica+An±Hm | (3),(4) |
| Mica+Qtz+Rk+Hm+An | (4) |
| Rk+Mt+An+Sd±Qtz* | (1) |

*very rare assemblage in a crocidolite band. Mode of occurrence: (1) crocidolite band, (2) massive riebeckite band, (3) thin layer (or lense) of fibrous to acicular riebeckite, (4) needle-like to prismatic riebeckite.
Abbreviations used throughout the text: Ac, acmite; An, ankerite; Hm, hematite; Ho, hornblende; Mi, minnesotaite; Mica, ferri-annite; Mt, magnetite; Pho, phosphate (apatite-like); Py, pyrite; Qtz, quartz; Rk, riebeckite; Sd, siderite; Stil, stilpnomelane.

The mode of occurrence of riebeckite may be classified as follows: (1) Crocidolite (fibrous variety of riebeckite) bands (mesobands) ranging from 2–150 mm thick; (2) Massive riebeckite bands (massive aggregates of fibrous to acicular riebeckite), ranging from 2–150 mm thick; (3) Thin layers (inclusive of veinlets) or lenses composed of fibrous to acicular riebeckite, generally less than 2 mm thick; and (4) Needle-like to prismatic riebeckite laths, dispersed in various mesoband matrices. Most of the riebeckite is concentrated in finely fibrous and massive bands. The other occurrences represent insignificant amounts. The textural types listed above are described in the following paragraphs.

### *Crocidolite bands*

Crocidolite seams are economically important, and their distribution and occurrence have been described in detail by Trendall and Blockley (1970). Crocidolite occurs as fracture fillings essentially parallel with the sedimentary banding. The long-fiber of the crocidolite tends to grow perpendicular to the bedding plane. Crocidolite mesobands commonly show swell and pinch structure and have poor lateral continuity. The contact between crocidolite-rich and other mesobands is generally sharp, and the crocidolite is often bounded by magnetite mesobands (1–5 mm thick), so called magnetite skins. Crocidolite is associated with magnetite, quartz, pyrite, and rarely ankerite and siderite. Small magnetite grains (<30 $\mu$m) are commonly dispersed through the bands. Quartz, with a fine, fibrous texture, occurs in parallel orientation with the crocidolite needles. Generally magnetite, quartz, and pyrite occur only in minor amounts within the crocidolite seams.

### *Massive riebeckite bands*

Such bands are composed mainly of interlocking aggregates of fibrous to acicular riebeckite. Lateral transitions from massive riebeckite to riebeckite-free banded iron-formation commonly occur without significant change in the pattern of individual mesobands (Eugster, 1969; Trendall and Blockley, 1970). According to Trendall and Blockley, magnetite mesobands in a riebeckite-free part can be traced into massive riebeckite but gradually die out in it. The riebeckite is associated with minor amounts of magnetite, hematite, and quartz, and locally small patches of stilpnomelane, ferri-annite, and ankerite. The assemblages of some bands are very similar to those of crocidolite bands. In places, euhedral magnetite or elongated hematite with grain sizes up to 50 $\mu$m may be abundant. Magnetite is generally less abundant (or absent) where hematite is present.

### *Thin layers or lenses*

Such riebeckite occurrences may be regarded as a smaller scale edition of massive riebeckite bands. However, the riebeckite here is more commonly associated with carbonates than in massive riebeckite bands. The layers are laterally discontinuous and commonly occur in chert-rich, carbonate-rich, and magnetite-rich bands (mesobands). They are composed of aggregates of fibrous to acicular riebeckite and small amounts of quartz, magnetite, pyrite, hematite, ankerite, siderite, stilpnomelane, and ferri-annite. Within chert-rich bands the riebeckite-rich layers may occur next to magnetite microbands; in such occurrences the riebeckite fibers appear as if they had grown on top of the magnetite. Riebeckite in carbonate (mainly ankerite)-rich bands is commonly associated with stilpnomelane and/or ferri-annite. Euhedral magnetite and/or pyrite may be dispersed within the layer. Needlelike to prismatic riebeckite commonly cuts such layers.

### *Needlelike to prismatic riebeckite*

Coarse individual grains of riebeckite (<50 $\mu$m in length and 100 $\mu$m in maximum width) are found in mesobands of chert, carbonate, quartz-iron oxide, and stilpnomelane. They are very scarce in mesobands of crocidolite or of massive riebeckite and may traverse thin bands and lenses composed of aggregates of fibrous to acicular riebeckite. Such coarse riebeckite is associated with quartz, carbonates (ankerite and siderite), magnetite, hematite, ferri-annite, and stilpnomelane. These coarse individual grains commonly coexist with carbonates. Texturally such grains appear to have grown on top of (at the expense of?) carbonate (especially ankerite) suggesting that ankerite played a role in the riebeckite formation.

### *Chemistry*

Representative chemical analyses of riebeckite from the Dales Gorge Member iron-formation, as determined by electron microprobe, are given in Table 2. The analyses can be described almost entirely by a combination of $Na_2O$, MgO, FeO, $Fe_2O_3$, $SiO_2$, and $H_2O$; all other components total less than one weight percent. The $Fe_2O_3$ content of the individual analyses was calculated on the assumption of solid solution only between the two end-members of riebeckite and magnesioriebeckite. With the aid of a computer program, a stoichiometric formula was calculated such that $Mg+Fe^{2+} = 3$ cations, and the remaining Fe was assigned to $Fe^{3+}$. The closeness of the approach of the trivalent octahedral cation sum to 2.00, shown in Table 2, supports the validity of this scheme. The composition of crocidolite is almost identical to that of massive riebeckite (Table 2, also see Trendall and Blockley, 1970; Miyano, 1976a). The $Fe^{2+}/(Fe^{2+}+Mg)$ ratio of riebeckite (hereafter simply referred to as Fe/(Fe+Mg)) shows some interesting aspects. The Fe/(Fe+Mg) ratios of minnesotaite and stilpnomelane tend to decrease with increasing $f_{O_2}$ at constant pressure and temperature (*e.g.*, Miyano 1978a,b,1982). The Fe/(Fe+Mg)(= $X_{Fe}^{Rk}$) of riebeckite, however, appears to be insensitive to an increase or decrease in oxygen fugacity. Similarly, the Fe/(Fe+Mg) ratio of ferri-annite formed contemporaneously with riebeckite is insensitive to such changes and appears to reflect that of the original stilpnomelane from which it formed (Miyano and Miyano, 1982). In the case of riebeckite, the ratio seems, however, to be influenced by the presence or absence of carbonates (Fig. 1). Representative microprobe analyses of associated carbonates are given in Table 3. Generally, the $X_{Fe}^{Rk}$ in

Table 2. Representative microprobe analyses of riebeckite in the Dales Gorge Member

| | 1<br>7Z142 | 2<br>10Z95 | 3<br>BF21 | 4<br>BF45 | 5<br>76B6 | 6<br>1M358 | 7 |
|---|---|---|---|---|---|---|---|
| $SiO_2$ | 53.00 | 52.90 | 53.85 | 54.43 | 54.34 | 53.48 | 52.18 |
| $Al_2O_3$ | 0.01 | 0.12 | 0.25 | 0.31 | 0.14 | 0.01 | 0.28 |
| $TiO_2$ | 0.00 | 0.57 | 0.00 | 0.10 | 0.15 | 0.01 | 0.02 |
| $Cr_2O_3$ | 0.00 | 0.04 | 0.00 | 0.04 | -- | -- | -- |
| $Fe_2O_3$* | 17.51 | 17.20 | 17.66 | 18.00 | 18.11 | 17.90 | 18.75 |
| FeO | 16.64 | 17.95 | 10.96 | 11.54 | 10.02 | 12.99 | 15.50 |
| MnO | 0.00 | 0.00 | 0.02 | 0.06 | 0.00 | 0.04 | 0.02 |
| NiO | 0.00 | 0.00 | 0.04 | 0.00 | -- | -- | -- |
| MgO | 3.92 | 2.96 | 7.23 | 7.16 | 8.10 | 6.27 | 3.82 |
| CaO | 0.12 | 0.12 | 0.08 | 0.18 | 0.26 | 0.05 | 0.53 |
| $Na_2O$ | 6.51 | 6.85 | 6.47 | 6.34 | 6.79 | 7.04 | 5.86 |
| $K_2O$ | 0.00 | 0.03 | 0.01 | 0.04 | 0.09 | 0.10 | 0.16 |
| $H_2O(+)$ | -- | -- | -- | -- | -- | -- | 2.50 |
| $H_2O(-)$ | -- | -- | -- | -- | -- | -- | 0.48 |
| total | 97.71 | 98.74 | 96.57 | 98.20 | 98.00 | 97.89 | 100.10 |
| | number of ions on the basis of 23 oxygens | | | | | | |
| Si | 8.021 | 7.976 | 8.020 | 7.991 | 7.962 | 7.967 | 7.944 |
| Al | 0.000 | 0.021 | 0.000 | 0.009 | 0.024 | 0.002 | 0.050 |
| Σ | 8.021 | 7.997 | 8.020 | 8.000 | 7.986 | 7.969 | 7.994 |
| Al | 0.002 | 0.000 | 0.044 | 0.045 | 0.000 | 0.000 | 0.000 |
| Ti | 0.000 | 0.065 | 0.000 | 0.011 | 0.017 | 0.001 | 0.002 |
| Cr | 0.000 | 0.005 | 0.000 | 0.005 | -- | -- | -- |
| $Fe^{3+}$ | 1.994 | 1.952 | 1.979 | 1.989 | 1.997 | 2.007 | 2.148 |
| $Fe^{2+}$ | 2.106 | 2.263 | 1.365 | 1.417 | 1.228 | 1.618 | 1.973 |
| Mn | 0.000 | 0.000 | 0.003 | 0.007 | 0.000 | 0.005 | 0.003 |
| Ni | 0.000 | 0.000 | 0.005 | 0.000 | -- | -- | -- |
| Mg | 0.884 | 0.665 | 1.605 | 1.567 | 1.769 | 1.393 | 0.867 |
| Σ | 4.986 | 4.950 | 4.996 | 5.041 | 5.011 | 5.024 | 4.993 |
| Ca | 0.019 | 0.019 | 0.013 | 0.028 | 0.041 | 0.008 | 0.086 |
| Na | 1.910 | 2.003 | 1.868 | 1.805 | 1.929 | 2.034 | 1.730 |
| K | 0.000 | 0.006 | 0.002 | 0.007 | 0.017 | 0.019 | 0.031 |
| Σ | 1.929 | 2.028 | 1.883 | 1.840 | 1.987 | 2.061 | 1.847 |
| Fe/Fe+Mg** | 0.823 | 0.864 | 0.676 | 0.685 | 0.646 | 0.722 | 0.833 |
| $X_{Fe}^{Rk}$ | 0.704 | 0.773 | 0.460 | 0.475 | 0.410 | 0.538 | 0.710 |

**estimated from total Fe assuming solid solution between riebeckite and magnesioriebeckite. **Molar ratio based on total Fe. --: not determined. 1: massive riebeckite, Rk+Hm+Mt±Qtz; 2: prismatic riebeckite, Stil+Mica+Mt+Rk+Ho+Qtz; 3: needle-like to prismatic riebeckite, Qtz+An+Rk+Mt+Hm; 4: thin layer of fibrous riebeckite, Rk+An+Mt+Py+Stil; 5: Massive riebeckite in contact with a carbonate band, Rk+An+Sd+Qtz+Hm+Mt+Stil; 6: prismatic riebeckite, Mica+Rk+An+Hm+Qtz; 7: crocidolite, average composition of 6 analyses taken from Trendall and Blockley (1970) and Miyano (1976a), Rk+Mt±Qtz±Py.*

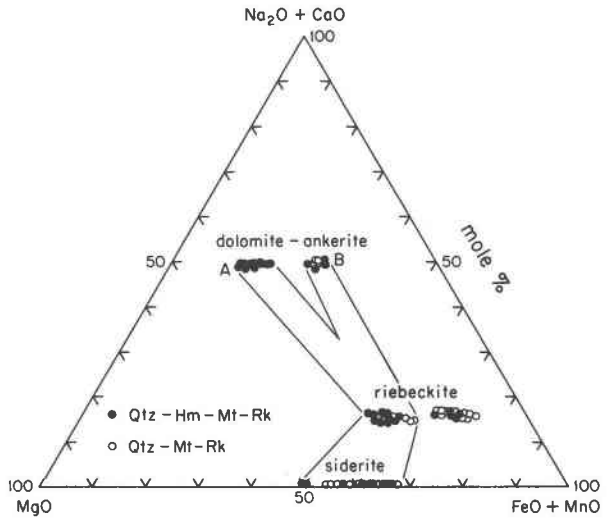


Fig. 1. Compositional diagram showing differences between carbonate-free and carbonate-bearing assemblages in the Dales Gorge Member. Total Fe as FeO. Compiled from compositional data in Tables 2 and 3 (this study) and Miyano (1982). Ankerite (B) may be a recrystallization product related to the formation of riebeckite. Subtracting estimated $Fe_2O_3$ from total FeO, (FeO+MnO) shifts positions of riebeckite analyses to 30.7–43.3% for carbonate-bearing assemblages and to 47.0–61.6% for caronate-free assemblages with ($Na_2O$+CaO) ranging from 23.7% to 26.2%.

crocidolite and massive riebeckite bands, where carbonates are virtually absent, ranges from 0.65 to 0.80. In contrast, this ratio, in carbonate-bearing assemblages, ranges from 0.40 to 0.55. Needlelike to prismatic riebeckite generally contains considerable Mg. The Fe/(Fe+Mg) ratios of the associated members of the dolomite-ankerite series are highly variable (see A and B in Fig. 1). This variability may be related to the recrystallization of the ankerite.

## Estimation of thermodynamic properties

Because thermodynamic properties for riebeckite are not available, they will be estimated by a combination of published methods for the prediction of entropy and Gibbs free energy, and through the evaluation of experimental data. Recently Helgeson *et al.* (1978) proposed a method for the estimation of the third-law entropy of silicate minerals, with a maximum uncertainty of about 1 percent. The estimated entropy of riebeckite by this method is 655.2 J/mol · °K. The standard Gibbs free energy of riebeckite can be estimated by Chen's (1975) method to be −9323.2 kJ/mol with the large uncertainty of ±63 kJ/mole. Furthermore, the hydrothermal data by Ernst (1962) can be used for an estimation of thermodynamic properties. Ernst experimentally determined the stability field of riebeckite (in which the degree of ordering among octahedral cations is unknown) over a range of oxygen fugacities at temperatures higher than about 470°C and pressures of up to 2 kbar. The equilibrium reaction on which the estimates are based is:

$$\underset{\text{riebeckite}}{2Na_2Fe_3^{2+}Fe_2^{3+}Si_8O_{22}(OH)_2} + \underset{\text{vapor}}{(m+n-2)H_2O} = \underset{\text{hematite}}{mFe_2O_3} + \underset{\text{magnetite}}{nFe_3O_4} + \underset{\text{acmite}}{4NaFe(SiO_3)_2} + \underset{\text{quartz}}{8SiO_2} + \underset{\text{vapor}}{(m+n)H_2} \quad (1)$$

where m and n are variable stoichiometric coefficients for hematite and magnetite, respectively, which are a function of how open the system is with respect to hydrogen. Acmite and riebeckite are considered to be nearly pure phases in the range of the hematite–magnetite buffer. The *P–T* brackets for this reaction obtained by Ernst (1962) are: (1) 469±5°C, 0.25 kbar; (2) 481±5°C, 0.5 kbar; (3) 496±5°C, 1 kbar; and (4) 515±5°C, 2 kbar. The pressure uncertainty is ±10 bars and is insignificant in the present calculations.

The two extreme sets of (m,n) are (0,2) and (3,0). Using Zen's method (1973) for buffered-hydrothermal data, the thermodynamic properties may be evaluated on the basis of Reaction (1) with two pairs of stoichiometric coefficients (0,2) and (3,0). Because heat capacity data are lacking for both riebeckite and acmite, the constant-entropy method must be employed:

Table 3. Representative microprobe analyses of carbonates coexisting with riebeckite in the Dales Gorge Member

| | 1 BF25 | 2 BF46 | 3 1B456 | 4 1M384 | 5 76B41 | 6 1B471 |
|---|---|---|---|---|---|---|
| FeO* | 20.53 | 19.48 | 15.87 | 16.59 | 48.22 | 42.66 |
| MnO | 0.05 | 0.03 | 0.03 | 0.99 | 0.14 | 0.04 |
| NiO | 0.07 | 0.07 | 0.00 | -- | -- | 0.00 |
| MgO | 8.38 | 8.82 | 11.35 | 10.83 | 10.55 | 14.65 |
| CaO | 27.52 | 27.48 | 28.28 | 28.20 | 0.17 | 0.07 |
| $Na_2O$ | 0.12 | 0.06 | 0.04 | 0.05 | 0.03 | 0.00 |
| Total | 56.67 | 55.94 | 55.57 | 56.66 | 59.11 | 57.42 |
| | recalculated on basis of 2 oxygens | | | | | |
| $Fe^{2+}$ | 0.580 | 0.553 | 0.439 | 0.454 | 1.431 | 1.238 |
| Mn | 0.001 | 0.001 | 0.001 | 0.027 | 0.004 | 0.001 |
| Mg | 0.442 | 0.446 | 0.559 | 0.529 | 0.558 | 0.758 |
| Ca | 0.996 | 1.000 | 1.001 | 0.989 | 0.006 | 0.003 |
| Σ | 1.999 | 2.000 | 2.000 | 1.999 | 1.999 | 2.000 |
| Fe/Fe+Mg | 0.579 | 0.553 | 0.440 | 0.462 | 0.719 | 0.620 |
| Fe/Fe+Mg+Mn | 0.578 | 0.553 | 0.439 | 0.450 | 0.718 | 0.620 |

**total iron as FeO. 1: ankerite coexisting with needle-like to prismatic riebeckite, Qtz+An+Rk+Mt+Hm; 2: ankerite in contact with a thin layer of fibrous riebeckite, Rk+An+Mt+Py+Stil±Qtz; 3: ankerite associated with massive riebeckite, Rk+An+Sd+Qtz+Hm+Mt±Stil; 4: ankerite associated with a mica-rich layer, Mica+Rk+An+Hm+Qtz; 5: siderite, same as 3; 6: siderite coexisting with a thin layer of fibrous riebeckite, Qtz+Rk+Sd+Hm+Mt.*

Table 4. Calculated values $\Delta G^\circ_f$ (Rk) - $2\Delta G^\circ_f$ (Ac) and $S'_f$ (Rk) - $2S'_f$ (Ac) from hydrothermal data (Ernst, 1962). See text for explanation.

| | | $\Delta G^\circ_f$(Rk)-$2\Delta G^\circ_f$(Ac) kJ, at 25°C | | $S'_f$(Rk)-$2S'_f$(Ac) J, at 25°C | |
|---|---|---|---|---|---|
| (m,n) | | (0,2) | (3,0) | (0,2) | (3,0) |
| Pair of brackets | | | | | |
| (2)&(3) | min | -4513.838 | -4517.381 | -1165.763 | -1165.349 |
| | max | -4518.240 | -4521.674 | -1173.104 | -1172.453 |
| (2)&(4) | min | -4514.172 | -4517.691 | -1166.505 | -1166.031 |
| | max | -4517.278 | -4520.758 | -1171.015 | -1170.457 |
| (3)&(4) | min | -4514.456 | -4517.950 | -1167.090 | -1166.570 |
| | max | -4516.462 | -4519.975 | -1169.367 | -1168.884 |
| mean | | -4515.741 | -4519.238 | -1168.807 | -1168.291 |
| (±1σ) | | (±1.836) | (±1.804) | (±2.869) | (±2.796) |

$$\Delta G_r(T,P) \simeq \Delta G^\circ_s(298,1) + \Delta V_s(P-1) - \Delta S'_s(298,1) \times (T-298.15) + (m+n)\mu_h - (m+n-2)\mu_w \quad (2)$$

where $\Delta G_r(T,P)$ is the Gibbs free energy change of Reaction (1) at temperature $T$ and pressure $P$. Subscript s means solid, and $\Delta G^\circ_s(298,1)$ and $\Delta V_s$, are, respectively, the Gibbs free energy change and the volume change for the solids of the reaction. $\Delta S'_s(298,1)$ is the formation-entropy change for the solids in the reaction; $\mu_h$ and $\mu_w$ are the chemical potentials for hydrogen and water, respectively, at $T$ and $P$. Equation (2) can be adapted to Reaction (1) as follows:

$$2\{\Delta G^\circ_f(Rk) - 2\Delta G^\circ_f(Ac)\} - 2\{S'_f(Rk) - 2S'_f(Ac)\}\Delta T = m\Delta G^\circ_f(Hm) + n\Delta G^\circ_f(Mt) + 8\Delta G^\circ_f(Qtz) - \{mS'_f(Hm) + nS'_f(Mt) + 8\,S'_f(Qtz)\}\Delta T + \Delta V_s\Delta P + (m+n)\mu_h - (m+n-2)\mu_w \quad (3)$$

where $\Delta G^\circ_f$ and $S'_f$ are the standard molar Gibbs free energy and entropy of formation from the elements of the mineral at 25°C, respectively. The right side of Equation (3), except for $\mu_h$ and $\mu_w$, can be evaluated using thermochemical data from Robie *et al.* (1978) and volume data from Robie *et al.* (1967) and Ernst (1968). Values for $\mu_h$ and $\mu_w$ can be calculated from data by Shaw and Wones (1964), Burnham *et al.* (1969), Huebner (1971), and Fisher and Zen (1971), assuming ideal mixing of water and hydrogen gas species. This leads to values of $\Delta G^\circ_f(Rk) - 2\Delta G^\circ_f(Ac)$ and $S'_f(Rk) - 2S'_f(Ac)$ from pairs of brackets: (2) and (3); (2) and (4); and (3) and (4); using the maximum and minimum values of the equilibrium temperatures. Bracket (1) was not used in the final calculations because the data from this bracket were not consistent with those at higher temperature. The results for the three pairs of brackets are given in Table 4. The mean values and their standard deviations are:

for (0,2)

$$\Delta G^\circ_f(Rk) - 2\Delta G^\circ_f(Ac) = -4515.741 \pm 1.836 \text{ kJ}$$
$$S'_f(Rk) - 2S'_f(Ac) = -1168.807 \pm 2.869 \text{ J}$$

for (3,0)

$$\Delta G^\circ_f(Rk) - 2\Delta G^\circ_f(Ac) = -4519.238 \pm 1.804 \text{ kJ}$$
$$S'_f(Rk) - 2S'_f(Ac) = -1168.291 \pm 2.796 \text{ J}$$

The above values for (0,2) and (3,0) are in fairly good agreement with each other. The best values of $\Delta G^\circ_f(Rk) - 2\Delta G^\circ_f(Ac)$ and $S'_f(Rk) - 2S'_f(Ac)$ are probably close to the mean values between (0,2) and (3,0). From the mean value of the free energy term in Table 4, the following relation can be evaluated,

$$\Delta G^\circ_f(Rk) = 2\Delta G^\circ_f(Ac) - 4517.5 \text{ (kJ)}. \quad (4)$$

The probable free energy values for acmite and riebeckite are illustrated in Figure 2 by superimposing the limits of error in the predicted free energies on the graphical expression of Equation (4). The predicted $\Delta G^\circ_f$(Ac) is −2434.3±21 kJ/mol (Chen's method). The figure shows that the free energy values lie between −2413.3 and −2434.4 kJ/mol for acmite and −9344.1 and −9386.2 kJ/mol for riebeckite. Taking into account the uncertainties in the calculation from the hydrothermal data (Table 4), the Gibbs free energies and their errors may be estimated as −9365.2±22 kJ/mol for riebeckite, and −2423.9±15 kJ/mol for acmite. The accuracy of this method could be improved by using a more reliably-predicted free energy value.

Similarly, the third-law entropies of acmite and riebeckite can be estimated. From the mean value of the entropy term in Table 4, one can evaluate

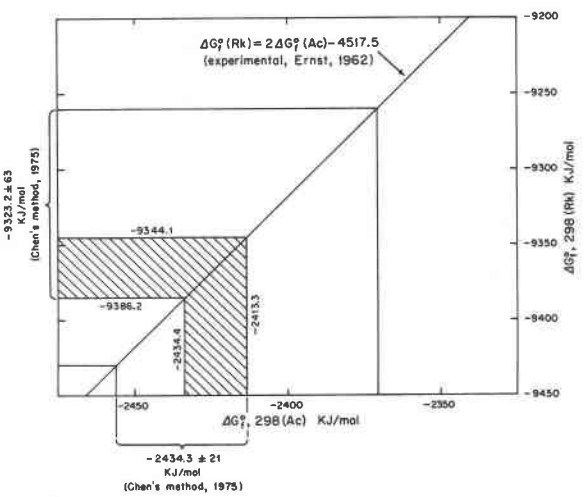


Fig. 2. Predicted range of standard free energies at 25°C, for riebeckite and acmite. Experimental data of Ernst (1962) for riebeckite and acmite were used in the estimates of the standard free energies at 25°C. The best fit (hatched area) is constrained by predicted values from Chen (1975) (see text).

$$S^\circ_f(\text{Rk}) = 2S^\circ_f(\text{Ac}) - 1168.55 \text{ (Joul)},$$

that is,

$$S^\circ(\text{Rk}) = 2S^\circ(\text{Ac}) + 350.12 \text{ (Joul)}. \quad (5)$$

Using a predicted entropy for acmite of 153.6 J/mol · K (Helgeson *et al.* 1978), $S^\circ$(Rk) becomes 657.3 J/mol · K. This value is in very good agreement with 655.2 J/mol · K of Helgeson *et al.* (1978). The error in the entropy of riebeckite is estimated as ±6 J/mol · K. The standard molar enthalpy values for riebeckite and acmite are then estimated to be −10058.30 and −2596.26 kJ/mol, respectively. The estimated values of the standard entropy, enthalpy, and Gibbs free energy of riebeckite may be compared with experimentally determined values for crocidolite which contains about 84 percent of the riebeckite end member (Bennington *et al.*, 1978); 674.0±17 J/mol · K, −10182.0±13 kJ/mol, and −9496.8 kJ/mol, respectively.

It is possible to determine the values of $S^\circ_f(\text{Rk}) - 2S^\circ_f(\text{Ac})$ and $\Delta G^\circ_f(\text{Rk}) - 2\Delta G^\circ_f(\text{Ac})$ using the estimated heat capacity ($C_p$) power functions of riebeckite and acmite (Helgeson *et al.* 1978). The $\Delta G^\circ_f(\text{Rk}) - 2\Delta G^\circ_f(\text{Ac})$ values for the two extreme sets of (m,n) differ by 3.7 kJ for (3,0) and 8.4 kJ for (0,2) from those evaluated from the constant-entropy method. Because both $C_p$ power functions involve hematite, but not magnetite, as a $C_p$ constituent, the uncertainties can be reduced by adjustment in the reaction for (3,0). A larger discrepancy for (0,2) may therefore reflect the presence of magnetite and absence of hematite. This may also be responsible for the large difference of $S^\circ_f(\text{Rk}) - 2S^\circ_f(\text{Ac})$ values for (0,2) in the two methods. As a result, the value for (0,2) evaluated from the $C_p$ power functions is probably not a good equivalent of that for (3,0) in estimating a mean value. The difference of the $\Delta G^\circ_f$ values for riebeckite in the two methods is up to 4 kJ/mole in the worst case. If the magnitude of the difference of $\Delta G^\circ_f(\text{Rk}) - 2\Delta G^\circ_f(\text{Ac})$ values for (0,2) in the two methods is assumed to be the same as that for (3,0), a final $\Delta G^\circ_f$ value of riebeckite is greater by only 2 kJ/mole than that calculated from the constant-entropy method. Because serious errors caused by the use of $C_p$ power functions are not expected in our present calculations, the thermodynamic properties of riebeckite (up to 500°C) have been estimated from the $C_p$ power functions, as shown in Table 5. The best estimate of such properties must, however, await more accurate $C_p$ power functions for riebeckite and acmite.

Table 5. Thermodynamic properties of riebeckite at elevated temperatures

| T(°C) | Cp(J/mol·K) | S°(J/mol·K) | ΔH°(kJ/mol)* |
|---|---|---|---|
| 25 | 696.34 | 657.30 | -10058.30 |
| 50 | 734.40 | 714.93 | -10040.40 |
| 100 | 793.40 | 824.95 | -10002.12 |
| 150 | 838.05 | 927.58 | -9961.29 |
| 200 | 874.09 | 1023.21 | -9918.46 |
| 250 | 904.64 | 1112.57 | -9873.98 |
| 300 | 931.54 | 1196.37 | -9828.06 |
| 350 | 955.90 | 1275.30 | -9780.86 |
| 400 | 978.45 | 1349.95 | -9732.50 |
| 450 | 999.68 | 1420.82 | -9683.04 |
| 500 | 1019.92 | 1488.32 | -9632.55 |

*based on the relation $\Delta H^\circ(T) = \Delta H^\circ_f(298) + \int_{298}^{T} Cp(T)dT$. The Cp of riebeckite was taken from Helgeson *et al.* (1978).

## Formation of riebeckite

Generally it is difficult to deduce probable reactions that took place during diagenesis or metamorphism of natural rocks, because one commonly deals with a multicomponent–multiphase system, and because of the presence of undetectable reactants and products such as ionic and fluid species. The following reactions for riebeckite formation are, however, predicted on the basis of textural relationships and mineral assemblages (Table 1; and Klein and Gole, 1981):

iron-oxides + quartz + $H_2O$ → riebeckite,

carbonates(siderite) + quartz + $H_2O$ → riebeckite + $CO_2$,

iron-oxides + carbonates + quartz + $H_2O$ → riebeckite + $CO_2$,

stilpnomelane + carbonates + quartz → riebeckite (+mica) + $CO_2$,

and stilpnomelane + iron-oxides → riebeckite (+mica).

In each of the above reactions, $Na^+$ and $K^+$ are required on the left side of the reaction. These alkali ions must have been supplied from somewhere in the rock system at the time of formation of the riebeckite.

The first three reactions appear to be important in the formation of riebeckite. The last two are less important, but significant because stilpnomelane is commonly replaced by ferri-annite near or within a riebeckite-rich zone (Miyano, 1982). Hematite and/or magnetite and quartz are the sources of iron and silica, respectively. Siderite (Fe/(Fe+Mg) = 0.50–0.85), dolomite–ankerite (0.20–0.65), and stilpnomelane (0.55–0.85) fix essentially all of the magnesium in the Dales Gorge Member banded iron-formation (compositional data: Ayres, 1972; Miyano, 1976a, 1978c, 1982; Miyano and Miyano, 1982). Because the Fe/(Fe+Mg) ratio of stilpnomelane is nearly the same as that of ferri-annite by which it is replaced (Miyano and Miyano, 1982), the carbonates may be a major source of magnesium as well as iron for riebeckite.

Generally riebeckite associated with carbonates has a higher MgO content (Fig. 1 and Table 2) than that of carbonate-free associations. Among the carbonates, siderite may be an important reactant during diagenesis because it is very scarce and dolomite-ankerite and calcite are more common in most riebeckite assemblages. The absence of siderite in riebeckite-bearing rocks was also noted by Klein and Gole (1981) in the Marra Mamba Iron Formation.

## Stability of riebeckite

On the basis of the general reactions for riebeckite formation noted above, possible reactions in the simple system Na–Fe–Si–C–O–H may be deduced as follows:

$$\text{riebeckite} + 2H^+ + 1/3\ O_2 = \tfrac{5}{3}\ Fe_3O_4 + 8SiO_2 + 2H_2O_{(l)} + 2Na^+, \quad (5)$$

$$\text{riebeckite} + 2H^+ + 3/4\ O_2 = \tfrac{5}{2}\ Fe_2O_3 + 8SiO_2 + 2H_2O_{(l)} + 2Na^+, \quad (6)$$

$$\text{riebeckite} + 5H_2CO_3 + 2H^+ = 5FeCO_3 + 8SiO_2 + 7H_2O_{(l)} + 2Na^+ + 1/2\ O_2, \quad (7)$$

$$\text{riebeckite} + 5HCO_3^- + 7H^+ = 5FeCO_3 + 8SiO_2 + 7H_2O_{(l)} + 2Na^+ + 1/2\ O_2, \quad (8)$$

$$\text{riebeckite} + 5CO_3^{2-} + 12H^+ = 5FeCO_3 + 8SiO_2 + 7H_2O_{(l)} + 2Na^+ + 1/2\ O_2. \quad (9)$$

For each of the above reactions the system is assumed to be saturated with respect to quartz. Using thermodynamic properties for minerals, $H_2O$, $O_2$ and ionic species from Robie *et al.* (1978), Helgeson *et al.* (1978), Miyano (1981), and the average heat capacities and dissociation constants for ionic species at elevated temperature from Criss and Cobble (1964a,b) and Helgeson (1967, 1969), the equilibrium constants of Reactions (5) to (9) can be calculated up to 300°C and are given in Table 6.

### *Carbonate-free assemblages*

Because values of $a_{Na^+}$ and $a_{H^+}$ (pH) at the time of riebeckite formation can not be specified, it is convenient to evaluate the stability relations among riebeckite, quartz, hematite, and magnetite in $\log f_{O_2} - \log a_{Na^+}/a_{H^+}$ diagrams at constant $T$ and in $\log f_{O_2}$ – pH space at constant $a_{Na^+}$ and $T$. The temperature of formation of riebeckite in diagenetic to very low-grade metamorphic iron-formations has been estimated to range from 100 to 150°C (*e.g.*, Trendall and Blockley, 1970; Miyano, 1976b, 1978a; Klein and Gole, 1981). Figure 3 (constructed with equilibrium constants of Reactions (5) and (6) listed in Table 6) shows the stability relations at these temperatures, with riebeckite stable at the high $a_{Na^+}/a_{H^+}$ side and low $f_{O_2}$ part of the diagram. Hematite–riebeckite assemblages are stable to the right side of points $D_1$ to $D_5$ in Figure 3. At points $D_1$ to $D_5$, four phases, hematite, magnetite, quartz, and riebeckite are stable. The diagram demonstrates that point $D_1$ moves to $D_5$ (dashed line) with increasing temperature. The $a_{Na^+}/a_{H^+}$ ratio of the location of points $D_1$ to $D_5$ is relatively insensitive to changes in temperature, $10^{3.56}$ at 100°C and $10^{3.84}$ at 150°C.

Table 6. Calculated equilibrium constants for riebeckite stability

| | Equilibrium constant (log K (T,1)) | | | | | | |
|---|---|---|---|---|---|---|---|
| Reaction | 25°C | 50°C* | 100°C | 150°C | 200°C | 250°C | 300°C |
| (5) | 29.87 | 28.01 | 25.13 | 23.00 | 21.50 | 20.29 | 19.38 |
| (6) | 59.49 | 54.89 | 47.64 | 42.16 | 38.01 | 34.67 | 31.98 |
| (7) | -19.94 | -18.67 | -17.12 | -16.41 | -16.12 | -16.24 | -16.67 |
| | (-8.83) | (-8.43) | (-8.25) | (-8.59) | (-9.13) | (-9.91) | (-10.89) |
| (8) | 11.82 | 13.32 | 15.13 | 17.24 | 19.28 | 21.91 | 27.63 |
| | (22.92) | (23.56) | (24.00) | (25.06) | (26.28) | (28.24) | (33.41) |
| (9) | 63.42 | 64.94 | 65.93 | 68.69 | 72.68 | 79.06 | 94.53 |
| | (74.52) | (75.19) | (74.80) | (76.51) | (79.68) | (85.39) | (100.31) |
| (10) | 10.94 | 8.94 | 6.02 | 3.99 | 2.80 | 2.08 | 1.58 |

*estimated by interpolation. Thermodynamic data for materials, except riebeckite, were taken from Criss and Cobble (1964a,b), Helgeson (1967,1969), Robie et al. (1978), Helgeson et al. (1978) and Miyano (1981). The data for riebeckite are from this study. Values in parentheses are based on the data for siderite from Helgeson et al. (1978).

It is assumed that riebeckite formed at constant tem-

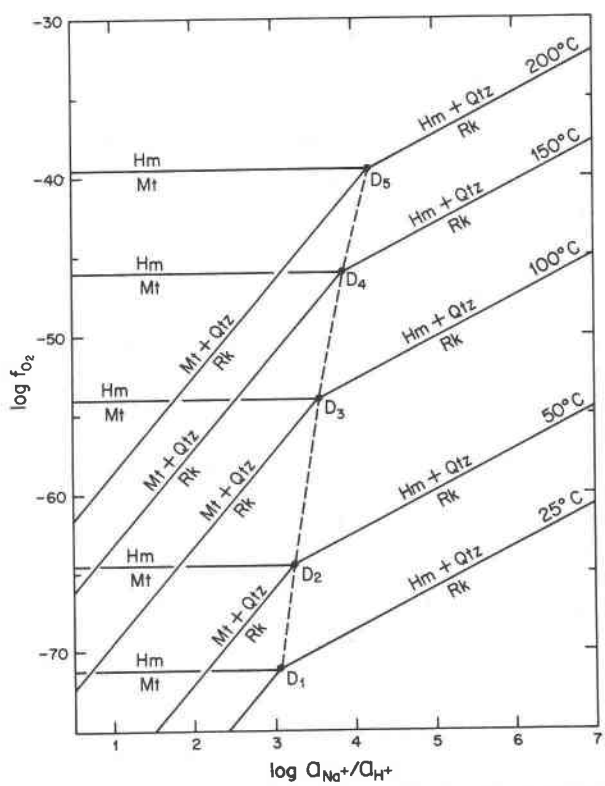


Fig. 3. Log $f_{O_2}$ - log $a_{Na^+}/a_{H^+}$ diagram showing the stability of riebeckite at various temperatures. Points $D_1$ to $D_5$ represent the assemblage Rk+Qtz+Mt+Hm. These points shift to slightly higher log $a_{Na^+}/a_{H^+}$ with increasing temperature.

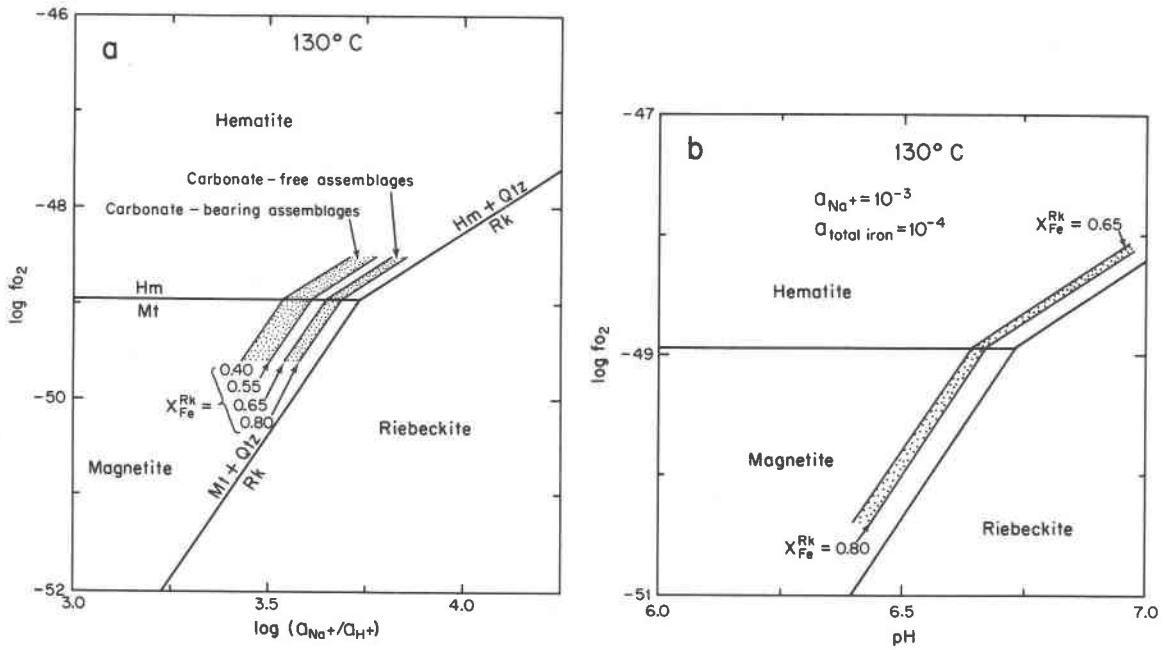


Fig. 4. Evaluation of Mg-substitution on riebeckite stability. *a*. Log $f_{O_2}$ - log $a_{Na^+}/a_{H^+}$ diagram at 130°C showing the location of riebeckite compositions in carbonate-free *vs*. carbonate-containing assemblages. The two dotted areas represent carbonate-free and carbonate-bearing assemblages with different $X^{Rk}{}_{Fe}$ values are shown. *b*. Log $f_{O_2}$ -pH diagram showing stability of Mg-poor riebeckite (in carbonate-free assemblages) at 130°C. The phase relations are similar to those in *a*. The riebeckite field moves to a higher pH with decreasing $a_{Na^+}$.

perature which is probably equivalent to the peak temperature of diagenesis or very-low grade metamorphism. Riebeckite formation must have been the result of intimate interaction of banded iron-formation with alkali-bearing solutions at that temperature. In subsequent diagrams, the temperature will be fixed at 130°C, as based on an estimate by Miyano (1978a).

According to Miyano (1976a,b), the $f_{O_2}$ during late diagenesis (or very low-grade metamorphism) of the Dales Gorge Member may have been largely controlled by the HM buffer. Oxygen buffering is also concluded to have taken place in the riebeckite-bearing rocks because the common association therein of hematite and magnetite. Crocidolite-rich bands, however, in which hematite is absent or rare and magnetite is common, may reflect $f_{O_2}$ conditions somewhat lower than those of the HM buffer.

In order to evaluate the effect of Mg substitution in riebeckite, an ideal solution model ($a^{Rk}_{Fe} = X^{Rk}_{Fe}$) between the end-members of riebeckite and magnesioriebeckite was used. Generally $X_{Fe}$ in Fe–Mg silicates increases with decreasing oxygen fugacity. In the Dales Gorge Member rocks (Fig. 1), $X^{Rk}_{Fe}$ in hematite-bearing associations is, however, not very different from that in hematite-free assemblages, but may in places be slightly higher in the latter. This is not contrary to the conclusion that the $f_{O_2}$ during metamorphism has been largely controlled by the HM buffer.

The estimated $f_{O_2}$ – $a_{Na^+}/a_{H^+}$ conditions, at constant temperature, applicable to the rocks of the Dales Gorge Member are shown within the dotted areas of Figure 4a. The conditions for the carbonate-free assemblages are located at higher $a_{Na^+}/a_{H^+}$ than those for the carbonate-bearing assemblages. At the HM buffer, the log $a_{Na^+}/a_{H^+}$ value is estimated to be 3.47 to 3.52 at 100°C (and 3.75 to 3.79 at 150°C) for the former and 3.36 to 3.43 at 100°C (and 3.64 to 3.71 at 150°C) for the latter. The results indicate that the effect of $X^{Rk}_{Fe}$ on the $a_{Na^+}/a_{H^+}$ ratio for the two types of assemblages is small at constant temperature. Because the effect of any variation in temperature or $f_{O_2}$ on $X^{Rk}_{Fe}$ is considered small, a high $X^{Rk}_{Fe}$ ratio for carbonate-bearing assemblages may be related to a lower $a_{Na^+}$ and/or higher $a_{total\ carbonate}$ of the solution, as will be discussed later.

Using the stability relations of riebeckite in a log $f_{O_2}$-pH diagram, at constant $a_{Na^+}$ ($10^{-2}$ to $10^{-4}$) and temperature (100 to 150°C), the effect of $X^{Rk}_{Fe}$ on $a_{Na^+}$ and pH in an alkali-bearing solution may be evaluated for carbonate-free assemblages. Assuming $a_{Na^+} = 10^{-3}$ (where riebeckite is stable at pH 6 to 7) and $a_{total\ Fe} \geq 10^{-4}$ (where hematite and magnetite are stable), the relations constructed at 130°C are shown in Figure 4b. The riebeckite field for the carbonate-free assemblages in the Dales Gorge Member is shown by the dotted area of the figure. For the assemblage hematite–magnetite–riebeckite, the pH values at the equilibrium point for that assemblage (see Fig. 4b) can be estimated at fixed $a_{Na^+}$ ($= 10^{-3}$). For

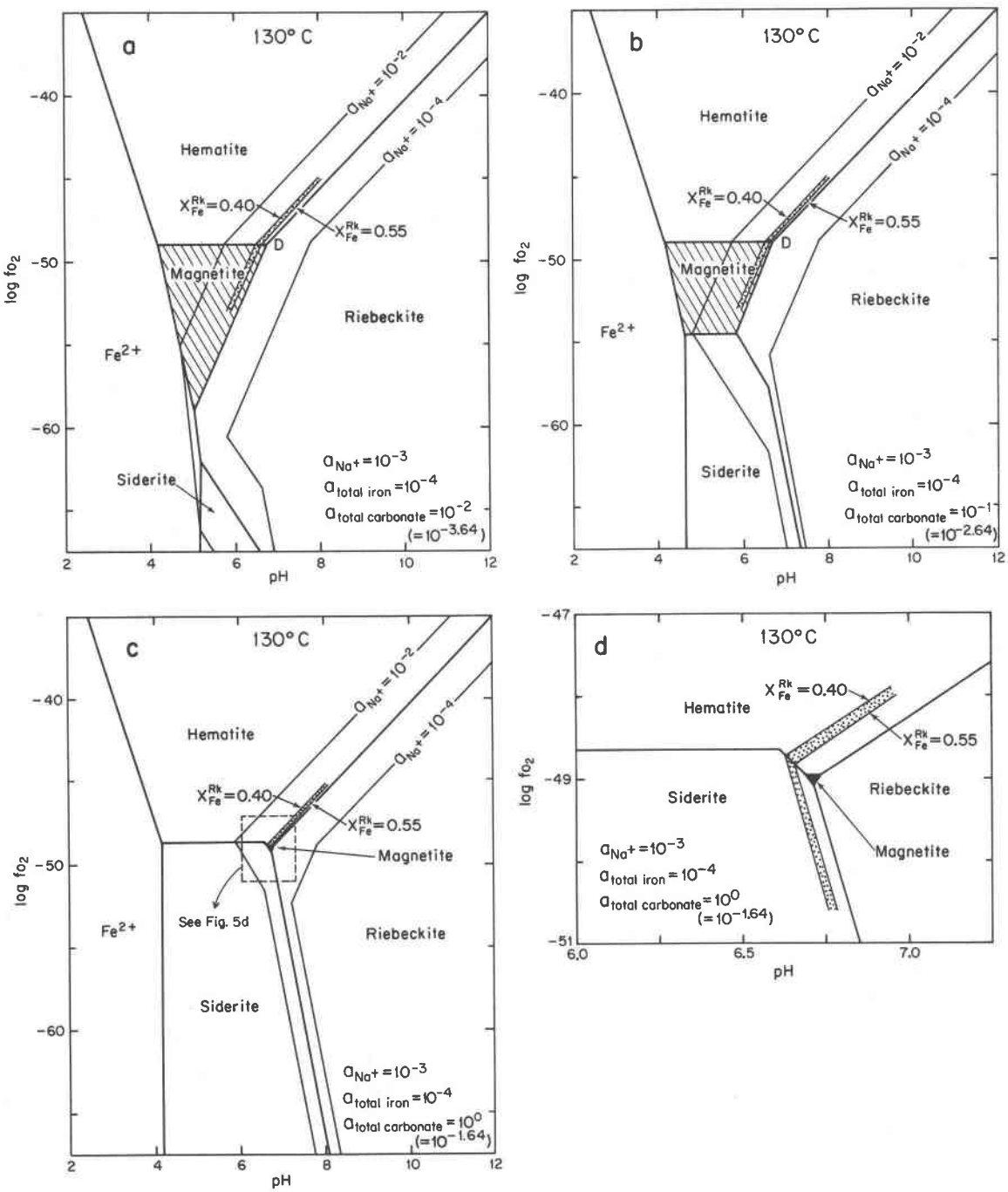


Fig. 5. Riebeckite–siderite stability relations. In these figures $a_{Na^+}$ is fixed at $10^{-2}$ to $10^{-4}$, and $a_{total\ Fe}$ at $10^{-4}$. The activity of total carbonate is fixed on the basis of thermodynamic data for siderite taken from Robie *et al.* (1978). The equivalent activity of total carbonate for the siderite data of Helgeson *et al.* (1978) is shown in parentheses. *A*. Log $f_{O_2}$-pH diagram at $a_{total\ CO_2} = 10^{-2}$ $(10^{-3.64})$, at 130°C. *B*. Log $f_{O_2}$-pH diagram at $a_{total\ CO_2} = 10^{-1}$ $(10^{-2.64})$, at 130°C. *C*. Log $f_{O_2}$-pH diagram at $a_{total\ CO_2} = 10^{0}$ $(10^{-1.64})$, at 130°C. *D*. Enlargement of central part of log $f_{O_2}$-pH diagram in Fig. 5C.

example, pH = 6.56 ($X_{Fe}^{Rk}$ = 1.0), 6.52 ($X_{Fe}^{Rk}$ = 0.8), and 6.47 ($X_{Fe}^{Rk}$ = 0.65) at 100°C; 6.84 ($X_{Fe}^{Rk}$ = 1.0), 6.79 ($X_{Fe}^{Rk}$ = 0.8), and 6.75 ($X_{Fe}^{Rk}$ = 0.65) at 150°C. Similarly one can evaluate the variation of $a_{Na^+}$ caused by a change of $X_{Fe}^{Rk}$. The $a_{Na^+}$ at constant $f_{O_2}$ and $T$ (100 to 150°C) varies slightly from $10^{-3.00}$ ($X_{Fe}^{Rk}$ = 1.0) to $10^{-3.04}$ ($X_{Fe}^{Rk}$ = 0.8) to $10^{-3.09}$ ($X_{Fe}^{Rk}$ = 0.65). These results show that a change in $X_{Fe}^{Rk}$ does not markedly affect the pH or $a_{Na^+}$ values of the

alkali-bearing solution. In other words, a slight change in pH or $a_{Na^+}$ of the solution may be responsible for the observed compositions of riebeckite, at fixed $f_{O_2}$ and temperature.

### *Carbonate-bearing assemblages*

The stability relations of carbonate-bearing assemblages may be evaluated using the equilibrium constants of Reactions (5) to (9) and of the following reactions,

$$\text{riebeckite} + 12\,H^+ = 2\,Na^+ + 5\,Fe^{2+} + 8SiO_2 + 7H_2O + \tfrac{1}{2}\,O_2, \quad (10)$$

$$Fe_2O_3 + 4\,H^+ = 2\,Fe^{2+} + 2H_2O + \tfrac{1}{2}\,O_2, \quad (11)$$

$$Fe_3O_4 + 6\,H^+ = 3\,Fe^{2+} + 3H_2O + \tfrac{1}{2}\,O_2, \text{ and} \quad (12)$$

$$FeCO_3 + 2\,H^+ = Fe^{2+} + H_2CO_3\ (pH < 6.6). \quad (13)$$

The equilibrium constants of Reactions (11) to (13) can be calculated from those of Reactions (5) to (10) listed in Table 6. Because of conflicting thermodynamic data for siderite (*e.g.*, compare Helgeson *et al.* (1978) with Robie *et al.* (1978)), the estimated stability relations are only qualitative.

The stability relations are expressed in log $f_{O_2}$-pH diagrams in Figure 5. In these diagrams, the activity of total iron is fixed at $10^{-4}$ and the activity of sodium ranges from $10^{-2}$ to $10^{-4}$. Three values of activity of total carbonate, $10^{-2}$, $10^{-1}$, and $10^{0}$, were chosen for the siderite data from Robie *et al.* (1978). They are equivalent to the data of Helgeson *et al.* (1978) of $10^{-3.64}$, $10^{-2.64}$, and $10^{-1.64}$, respectively. In these diagrams several assumptions were made with regard to the activities of ionic species. The activity of total iron (mostly $Fe^{2+}$, Miyano 1981) was fixed at $10^{-4}$ assuming that iron-oxides are stable within almost the entire range of pH. This activity decreases with increasing pH, at constant $f_{O_2}$. The range of sodium activity ($a_{Na^+}$) was chosen for an intermediate pH (about 5 to 8 at 130°C). The $a_{Na^+}$ in equilibrium with riebeckite increases with decreasing pH at constant $f_{O_2}$.

The effect of Mg substitution in siderite cannot be evaluated because of the ambiguous thermodynamic data for siderite. Such an effect may be of little significance because much of the siderite may have been precipitated prior to riebeckite formation.

In Figures 5a to c, the size of the siderite field is a function of the activity of total carbonate ($a_{\text{total } CO_2}$). In Figures 5a and b, riebeckite is not associated with siderite in the presence of hematite. The area of point D in Figures 5a and b may represent the conditions of carbonate-free assemblages, at a relatively small $a_{\text{total } CO_2}$. The effect of substitution of Mg ($X_{Fe}^{Rk}$ = 0.40 to 0.55) in riebeckite associated with carbonates is shown in Figures 5a to d by the slight shift (dotted region) from the pure phase lines to a lower pH. When one compares the various diagrams of Figure 5 it becomes clear that, for coexisting siderite and riebeckite, a decrease in $a_{Na^+}$ may be compensated by reduction in $X_{Fe}^{Rk}$ and an accompanying increase in $a_{\text{total } CO_2}$ at constant $f_{O_2}$.

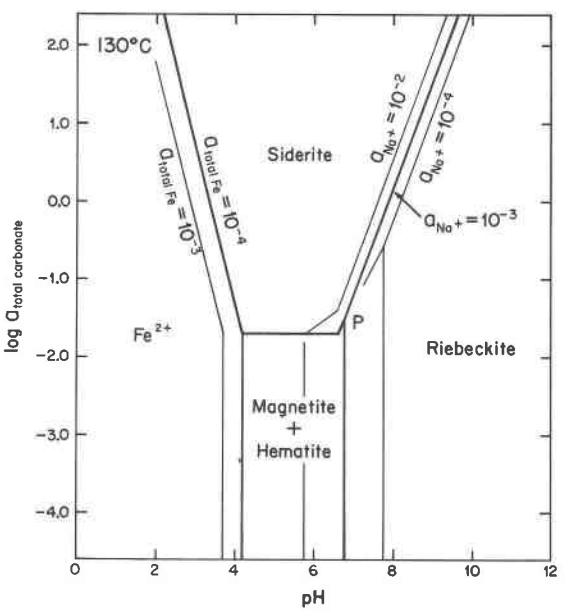


Fig. 6. Log $a_{\text{total } CO_2}$-pH diagram showing the stability relations of riebeckite and siderite at the HM buffer at 130°C. $a_{Na^+}$ and $a_{\text{total Fe}}$ are fixed at $10^{-2}$ to $10^{-4}$ and at $10^{-3}$ to $10^{-4}$, respectively. The stability field of siderite was determined on the basis of thermodynamic data from Helgeson *et al.* (1978). Point P ($a_{Na^+} = 10^{-3}$) represents minimum values for pH and $a_{\text{total } CO_2}$ for the riebeckite–siderite coexistence at the HM buffer.

## Possible mechanism of riebeckite formation

The previous discussion on riebeckite stability shows that major factors controlling riebeckite formation are $f_{O_2}$, $a_{Na^+}$, and $a_{\text{total } CO_2}$, at a given temperature. The $f_{O_2}$ is probably defined close to the HM buffer as previously noted. A mechanism of riebeckite formation can, therefore, be depicted as a function of $a_{Na^+}$ and $a_{\text{total } CO_2}$. If it is assumed that any variation in $a_{Na^+}$ during formation is small, it is possible to use a log $a_{\text{total } CO_2}$ − pH diagram as shown in Figure 6. A minimum for both the pH and $a_{\text{total } CO_2}$ for the association of siderite and riebeckite, is shown at point P ($a_{Na^+} = 10^{-3}$). This figure is, however, not applicable to those occurrences where siderite is absent. Because riebeckite is more commonly associated with ankerite instead of siderite, one may assume that ankerite is stable at lower $a_{\text{total } CO_2}$ than siderite as suggested in Figure 7. This figure, constructed on the basis of Figure 6, shows schematic phase relations involving ankerite, at constant $a_{Ca_{2+}}$ and at the HM buffer. On the basis of this diagram, a tentative evaluation of riebeckite formation may be developed. Before the availability of alkali-bearing solutions for the formation of riebeckite, the pH and $a_{\text{total } CO_2}$ (or equivalent $P_{CO_2}$) in the iron-formation system may have been at A in Figure 7. The alkali-bearing solutions would have had a sufficient

content of $Na^+$ for riebeckite formation and may well have been deficient in (or undersaturated with) carbonate species. The activity–pH conditions for such a solution are located at B (at an arbitrary pH). The change in $a_{\text{total CO}_2}$ from A to B may have been brought about by a sudden decrease in $P_{CO_2}$ through a deformational mechanism, such as microfracturing. Trendall and Blockley (1970) concluded from their petrographic studies that riebeckite formation is intimately related to evidence of deformation. According to Miyano (1978b,c), the $P_{CO_2}$ during diagenesis (or burial metamorphism) of the Dales Gorge Member and before formation of riebeckite, was about 5 to 20 bars, which is higher than that of other iron-formations associated with similar diagenetic to low grade metamorphic $P$–$T$ conditions. Although crocidolite of the Dales Gorge Member is stable somewhat below the HM buffer, massive riebeckite and crocidolite with a high $X_{Fe}^{Rk}$ may well have formed in a region between B and C, near the buffer. As a result of the reaction with the carbonates in the iron-formation and the formation of Fe-rich riebeckite, the initial solution may gradually have changed to a higher content of carbonate species and a lower content of $Na^+$. Crystallization of riebeckite associated with carbonates would have started at C (arbitrary pH) and ended at D (arbitrary pH), with increasing $a_{\text{total CO}_2}$. In Figure 7, the direction B to C to D is one of increase in both the activities of $Na^+$ and total carbonate. However, $a_{Na^+}$ of the solution may well have decreased as a result of riebeckite formation. Such a decrease in $a_{Na^+}$ is compensated to some extent by a decrease in $X_{Fe}^{Rk}$.

In summary, the formation of riebeckite (exclusive of the fibrous variety, crocidolite) suggests that alkali-bearing solutions have interacted with the iron-formations and have gradually changed toward a higher content of carbonate species and lower content of $Na^+$. It is probable that $a_{\text{total carbonate}}$ in the solution increased to the minimum value necessary for ankerite stability. On the other hand, the formation of crocidolite may have been the result of fracture filling by solutions in response to deformational mechanisms. It is likely that these solutions had a lower content of carbonate species and a higher content of $Na^+$ than those involved in riebeckite formation.

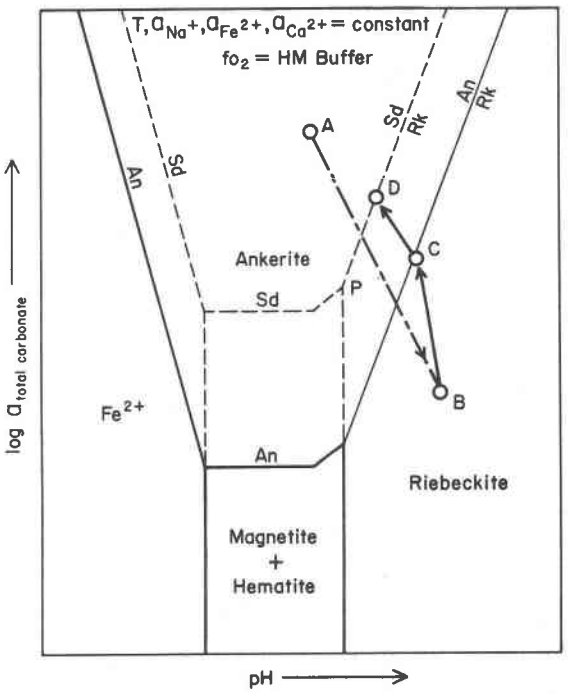


Fig. 7. Schematic log $a_{\text{total CO}_2}$-pH diagram showing the stability relations of riebeckite and ankerite at the HM buffer, at constant temperature. Ankerite is assumed to be stable at lower $a_{\text{total CO}_2}$ than siderite (see text). A possible mechanism of formation of riebeckite may follow path A→B→C→D (see text).

## Conclusions

On the basis of estimated thermodynamic properties of riebeckite, and on chemical and petrologic data, the stability relations of riebeckite have been quantitatively assessed in the system Na–Fe–Mg–Si–C–O–H. The relations in this system are applicable to an estimation of the physicochemical conditions for riebeckite formation in very low-grade metamorphic (or diagenetic) iron-formations. Some of the riebeckite occurrences in the Dales Gorge Member can be explained tentatively in terms of the estimated stability relations. The phase relations, however, are inconclusive and rather qualitative for carbonate-bearing assemblages because of a lack of available data. In the naturally occurring assemblages, $K^+$ ions have also played an important role as they are responsible for the crystallization of ferri-annite, which is commonly contemporaneous with riebeckite.

## Acknowledgments

This research was made possible by NSF grant EAR-8020377 (to C.K.), while the first author was on leave from the University of Tsukuba, Japan. Some additional funds were also made available by Indiana University, through the University Research and Operations Committee and the Department of Geology. An evaluation of the field relations of riebeckite in the Hamersley Group of Western Australia was made possible for C.K. through a Guggenheim Fellowship in 1978. Electron probe analyses were obtained at the Analytical Center of the University of Tsukuba and T.M. is grateful to N. Nishida for his help. We thank W. H. Moran, R. T. and Barbara Hill, and G. Ringer for the drafting and photography of the illustrations. We are grateful to Mrs. Thea Brown for the careful and expert typing of the manuscript and tables, and to W. G. Ernst and Frank S. Spear for their critical and constructive reviews of an earlier version of this manuscript.

## References

Ayres, D. E. (1972) Genesis of iron-bearing minerals in banded iron formation mesobands in the Dales Gorge Member. Economic Geology, 67, 1214–1233.

Bennington, K. O., Ferrante, M. J., and Stuve, J. M. (1978) Thermodynamic data on the amphibole asbestos minerals amosite and crocidolite. U. S. Bureau of Mines, Report of Investigations 8265.

Beukes, N. J. (1973) Precambrian iron-formations of southern Africa. Economic Geology, 68, 960–1004.

Beukes, N. J. (1980) Lithofacies and stratigraphy of the Kuruman and Griquatown iron-formations, northern Cape Province, South Africa. Transactions, Geological Society of South Africa, 83, 69–86.

Burnham, C. W., Holloway, J. R. and Davis, N. F. (1969) Thermodynamic properties of water to 1,000°C and 10,000 bars. Geological Society of America, Special Paper 132.

Chen, C. (1975) A method of estimation of standard free energies of formation of silicate minerals at 298.15°K. American Journal of Science, 175, 801–817.

Cilliers, J. J. le R. and Genis, J. H. (1964) Crocidolite asbestos in the Cape Province. In S. H. Haughton, Ed., The Geology of Some Ore Deposits in Southern Africa, vol. 2, p. 543–570. Geological Society of South Africa.

Criss, C. M. and Cobble, J. W. (1964a) The thermodynamic properties of high temperature aqueous solutions. IV. Entropies of the ions up to 200° and the correspondence principle. Journal of the American Chemical Society, 86, 5385–5390.

Criss, C. M. and Cobble, J. W. (1964b) The thermodynamic properties of high temperature aqueous solutions. V. The calculation of ionic heat capacities up to 200°: Entropies and heat capacities above 200°. Journal of the American Chemical Society, 86, 5390–5393.

Dimroth, E. and Chauvel, J. J. (1973) Petrography of the Sokoman Iron Formation in part of the central Labrador Trough, Quebec, Canada. Geological Society of America Bulletin 84, 111–134.

Du Toit, A. L. (1945) The origin of the amphibole asbestos deposits of South Africa. Transactions Geological Society of South Africa, 48, 161–206.

Ernst, W. G. (1962) Synthesis, stability relations, and occurrence of riebeckite and riebeckite–arfvedsonite solid-solutions. Journal of Geology, 70, 689–736.

Ernst, W. G. (1968) Amphiboles: Crystal chemistry, phase relations and occurrence. Springer-Verlag, New York.

Eugster, H. P. (1969) Inorganic bedded cherts from the Magadi area, Kenya. Contributions to Mineralogy and Petrology, 22, 1–31.

Fisher, J. R. and Zen, E. (1971) Thermochemical calculations from hydrothermal phase equilibrium data and the free energy of $H_2O$. American Journal of Science, 270, 297–314.

Genis, J. H. (1964) The formation of crocidolite asbestos. In S. H. Haughton, Ed., The Geology of Some Ore Deposits in Southern Africa, vol. 2, p. 571–578. Geological Society of South Africa.

Grubb, P. L. C. (1971) Silicates and their paragenesis in the Brockman Iron Formation of Wittenoom Gorge, Western Australia. Economic Geology, 66, 281–292.

Hall, A. L. (1930) Asbestos in the Union of South Africa. South Africa Geological Survey, Memoir 12.

Helgeson, H. C. (1967) Thermodynamics of complex dissociation in aqueous solution at elevated temperatures. Journal of Physical Chemistry, 71, 3121–3136.

Helgeson, H. C. (1969) Thermodynamics of hydrothermal systems at elevated temperatures and pressures. American Journal of Science, 267, 729–804.

Helgeson, H. C., Delany, J. M., Nesbitt, H. W., and Bird, D. K. (1978) Summary and critique of the thermodynamic properties of rock-forming minerals. American Journal of Science, 178-A, 1–229.

Huebner, J. S. (1971) Buffering techniques for hydrostatic systems at elevated pressures. In G. C. Ulmer, Ed., Research Techniques for High Pressure and High Temperature, p. 123–177. Springer-Verlag, New York.

Klein, C. (1974) Greenalite, stilpnomelane, minnesotaite, crocidolite and carbonates in a very low-grade metamorphic Precambrian iron-formation. Canadian Mineralogist, 12, 475–498.

Klein, C. and Gole, M. J. (1981) Mineralogy and petrology of parts of the Marra Mamba Iron Formation, Hamersley Basin, Western Australia. American Mineralogist, 66, 507–525.

Miles, K. R. (1942) The blue asbestos bearing banded iron formations of the Hamersley Ranges, Western Australia. Western Australia Geological Survey Bulletin 100.

Milton, C., Ingram, B., and Breger, I. (1974) Authigenic magnesioarfvedsonite from the Green River Formation, Duchesne County, Utah. American Mineralogist, 59, 830–836.

Miyano, T. (1976a) Mineral assemblages of the Proterozoic banded iron formation in the Hamersley area, Western Australia (in Japanese with English abstract). Mining Geology of Japan, 26, 273–288.

Miyano, T. (1976b) Physicochemical environments during burial metamorphism of the Dales Gorge Member, Hamersley Group, Western Australia (in Japanese with English abstract). Mining Geology of Japan, 26, 311–325.

Miyano, T. (1978a) Phase relations in the system Fe–Mg–Si–O–H and environments during low-grade metamorphism of some Precambrian iron formations. Journal of the Geological Society of Japan, 84, 679–690.

Miyano, T. (1978b) Stability relations of iron-bearing minerals in the $H_2O$–$CO_2$ mixed volatile region at lower temperatures. Journal of the Geological Society of Japan, 84, 711–719.

Miyano, T. (1978c) Effect of $CO_2$ on mineralogical differences in some low-grade metamorphic iron formations. Geochemical Journal, 12, 201–211.

Miyano, T. (1981) Examination of thermodynamic properties and stability relations of aqueous iron species at 25°C. Institute of Geoscience, University of Tsukuba, Science Reports (section B), 2, 61–76.

Miyano, T. (1982) Stilpnomelane, iron-rich mica, K-feldspar and hornblende in banded iron-formation assemblages of the Dales Gorge Member, Hamersley Group, Western Australia. Candian Mineralogist, 20, 189–202.

Miyano, T. and Miyano, S. (1982) Ferri-annite from the Dales Gorge Member iron-formation, Wittenoom area, Western Australia. American Mineralogist, 67, 1179–1194.

Robie, R. A., Bethke, P. M., and Beardsley, K. M. (1967) Selected X-ray Crystallographic Data, Molar Volumes, and Densities of Minerals and Related Substances. U. S. Geological Survey Bulletin 1248.

Robie, R. A., Hemingway, B. S., and Fisher, J. R. (1978) Thermodynamic properties of minerals and related substances at 298.15 K and 1 bar ($10^5$ Pascals) pressure and at higher temperatures. U. S. Geological Survey Bulletin 1452.

Shaw, H. R. and Wones, D. R. (1964) Fugacity coefficients for hydrogen gas between 0° and 1000°C for pressures to 3,000 atm. American Journal of Science, 262, 918–929.

Trendall, A. F. (1965) Progress report on the Brockman Iron

Formation in the Wittenoom–Yampire area. Western Australia Geological Survey Annual Report, 1964, 55–65.

Trendall, A. F. (1966) Second progress report on the Brockman Iron Formation in the Wittenoom–Yampire area. Western Australia Geological Survey Annual Report, 1965, 75–87.

Trendall, A. F. and Blockley, J. G. (1970) The iron formations of the Precambrian Hamersley Group, Western Australia with special reference to the associated corcidolite. Western Australia Gelogical Survey Bulletin 119.

Zajac, I. S. (1974) The stratigraphy and mineralogy of the Sokoman Formation in the Knob Lake area, Quebec and Newfoundland. Canadian Geological Survey Bulletin 220.

Zen, E. (1973) Thermochemical parameters of minerals from oxygen-buffered hydrothermal equilibrium data: method, application to annite and almandine. Contributions to Mineralogy and Petrology, 39, 65–80.

*Manuscript received, March 17, 1982;*
*accepted for publication, December 20, 1982.*